

Interaction of Synthetic Jets with Laminar and Turbulent Boundary Layers

Xin Wen and Hui Tang

School of Mechanical and Aerospace Engineering, Nanyang Technological University, Singapore 639798

Abstract

The interaction between circular synthetic jets and flat-plate laminar/turbulent boundary layers is investigated using CFD simulations in this study. For turbulent boundary layer simulations, large eddy simulation (LES) is applied so as to obtain more accurate flow details. The simulation results are validated using both existing experimental data and numerical results obtained from other researchers, and reasonable agreements are achieved. The simulated vortical structures produced by a circular synthetic jet issued into a laminar boundary layer and a turbulent boundary layer are analysed and compared. Obvious difference is found between the vortical structures formed in those two boundary layers. Meanwhile the effects of the different vortical structures on wall shear stresses are also evaluated to help identify the flow control effectiveness of synthetic jets in different types of boundary layers.

Introduction

A synthetic jet actuator (SJA), which is also known as a zero-net-mass-flux (ZNMF) actuator, consists of a cavity with an oscillatory diaphragm on its bottom side and an orifice on the opposite side. The periodic downward and upward motion of the diaphragm generates a succession of vortex structures that propagate away from the orifice, forming a so-called “synthetic jet”, as shown in Figure 1. Synthetic jets are regarded as a promising method for active flow separation control due to their ability to inject momentum to external flow without net mass flux.

There has been intense research on synthetic jets since 1990s [1,2,4] driven by the potential application of synthetic jets in delaying boundary layer separation on aircraft. It has been demonstrated in laboratory experiments and numerical simulations that synthetic jets are capable of delaying flow separation on aerodynamic bodies of various shapes [1,6,11]. Existing experimental and numerical evidence shows that the interaction of the train of vortices formed out of a circular synthetic jet with a local boundary layer induces streamwise vortical structures, which entrain faster moving fluid from the freestream to the near-wall region and are hence capable of delaying boundary layer separation. It was observed that, depending on the jet-to-freestream velocity ratio, different vortical structures are produced by the interaction between synthetic jets and boundary layers. As the velocity ratio increases, the primary structures first appear as hairpin vortices near the wall, then as stretched vortex rings moving towards the edge of boundary layer, and finally as distorted vortex rings which penetrate the edge of the boundary layer quickly [9]. Although a large amount of work has been done on investigating these coherent vortex structures in many aspects, to the best knowledge of the authors, most of the previous work focused on synthetic jets only in laminar boundary layers. However, in real-world applications, turbulent boundary layers are more common, and the difference in the behaviours of synthetic jets in laminar and turbulent boundary layers still remains an interesting and

untouched topic. In the numerical study reported in this paper, a circular synthetic jet is issued into both laminar and turbulent boundary layers, and the different behaviours of the resulting flow structures are compared. Upon validations of the CFD model using existing experimental data and numerical results obtained from other researchers, the simulation results are used to provide detailed information about vortical structures as well as the pattern of wall shear stress.

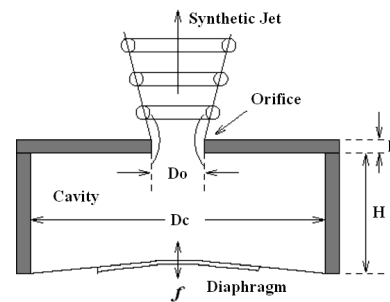


Figure 1. Schematic of a synthetic jet actuator (Zhong et al [8])

Computational Methods

Geometry and boundary conditions

The cavity of the SJA used in this numerical study has a diameter of $D_c = 45\text{mm}$ and a height of $H = 25\text{mm}$. Its orifice has a diameter of $D_o = 5\text{mm}$ and a height of $h = 5\text{mm}$, and its diaphragm oscillates in a sinusoidal manner. The reference position, $x = 0$, $y = 0$, and $z = 0$, is set as the axial centre of the orifice. The same freestream and jet velocities will be used in both the laminar and turbulent simulations. The geometry and boundary conditions for the laminar simulation are shown in Figure 2. Since the laminar flow field is expected to be symmetric relative to the central plane of the orifice, only a half of the flow field is simulated which is validated by Zhou and Zhong [10]. Both the orifice duct and the actuator cavity are included in the simulations and a velocity boundary condition instead of a moving boundary condition is applied at the neutral position of the diaphragm. The moving velocity of diaphragm can be expressed as

$$v(r, t) = \pi \Delta f \cos(2\pi f t) \quad (1)$$

where Δ is the peak-to-peak displacement of the diaphragm, and f is the oscillation frequency of diaphragm. For the laminar simulations, the Reynolds number based on momentum thickness is $Re_\theta = 180$, and the boundary layer thickness is about 3 times of the orifice diameter. For the turbulent simulations, the Reynolds number is $Re_\theta = 420$, and the boundary layer thickness is about 6 times of the orifice diameter. Since the flow cannot be assumed as symmetric, the entire domain is used in the turbulent simulations. Based on the dimensional analysis [9], the behaviour of synthetic jets issued into a given boundary layer is greatly determined by the jet-to-freestream velocity ratio, V/R , and the

Reynolds number based on the stroke length, Re_L . The jet-to-freestream velocity ratio is defined as

$$VR = \frac{\bar{U}_o}{U_\infty} \quad (2)$$

where U_∞ is the freestream velocity and \bar{U}_o is the time-averaged blowing velocity over an entire actuation cycle. And the Re_L based on the stroke length is defined as

$$Re_L = \frac{\bar{U}_o L_o}{\nu} \quad (3)$$

where L_o is the stroke length, which, according to the slug model [4], represents the length of the fluid column expelled during the blowing stroke. ν is the kinematic viscosity of water.

The freestream velocity of water at the inlet is fixed at $U_\infty = 0.1$ m/s in this study. The peak-to-peak displacement of the diaphragm is $\Delta = 0.106$ mm and the oscillating frequency is $f = 2$ Hz. These conditions yield that $VR = 0.17$ and $Re_L = 145$.

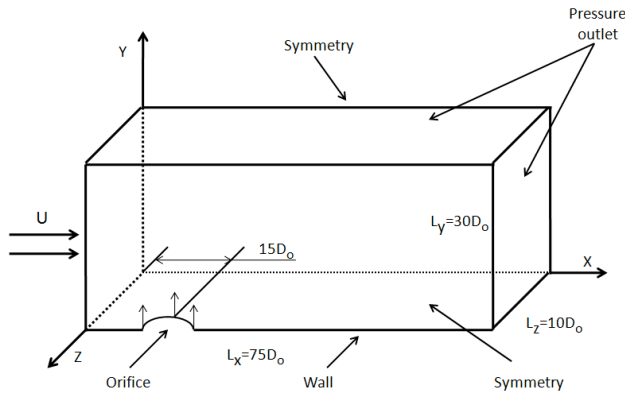


Figure 2. Computational geometry and boundary conditions for the laminar simulation case

Numerical solver

The commercial CFD software, ANSYS FLUENT 13.0, is used to solve unsteady 3D incompressible Navier-Stokes equations. In the laminar simulations, the Navier-Stokes equations are discretized by a second-order implicit scheme in time and a second-order upwind scheme in space. Pressure-Implicit with Splitting of Operators (PISO) method is used for pressure-velocity coupling. About 1.9 million mesh cells and 120 time steps per actuating cycle are used.

In the turbulent simulations, LES is applied by filtering the Navier-Stokes equations. The Wall-Adapting Local Eddy-Viscosity (WALE) Model is used for the approximation of the subgrid scale stress (SGS) terms. The filtered governing equations are discretized in space using a bounded central differencing scheme. The turbulent boundary layer is resolved with $y^+ \approx 0.5$ in wall-normal direction, and with both the streamwise and spanwise resolutions being $x^+ \approx 1$ and $z^+ \approx 1$ in the wake of the jet for the fine grid. About 4 million mesh cells and 120 time steps per actuating cycles are used. The freestream mean velocity at the inlet is adjusted to achieve the Reynolds number $Re_\theta = 420$. Vortex method [3] is used to generate a time-dependent velocity inlet boundary condition. The turbulent intensity is set 3% of the freestream velocity at the inlet. The entire domain is used in the simulation. The boundary conditions in the LES simulation are the same as those in the laminar simulations.

Validation of computational models

To validate the laminar simulation model, the reproduction of Zhou and Zhong's simulation results [10] is conducted. Both the phase-averaged and time-averaged velocity profiles at $x = 3D_o$ on the mid-span plane are compared between the results from the current simulation and those from Zhou and Zhong [10], as shown in figure 3. It can be seen that the profiles from the current simulation agree with the computed results and measured data in [10] well. Therefore, the current laminar simulation model is believed to be capable of simulating the interaction between synthetic jets and a laminar boundary layer.

For the LES simulations, before enabling the synthetic jet, the background flow of a turbulent boundary layer is firstly simulated. The simulated mean velocity profile at $x=0$ is compared with the test data provided by Zhong from University of Manchester. And the profiles of the normalized velocity fluctuations are compared with the DNS results with $Re_\theta = 300$ from Spalart [5]. As shown in figure 4a, a reasonably good agreement is achieved in the comparison of mean velocity profiles, demonstrating the capability of the current LES model in predicting mean velocity profiles for turbulent boundary layers. Although as shown in figure 4b significant discrepancies appear in the comparison of the velocity fluctuation profiles, especially for streamwise fluctuations u'^+ , the simulation is able to capture the key features of the three profiles in terms of the variation trends, the peak values, and the location of the fluctuation peaks. The agreements in near wall region are particularly good, meaning that the current mesh density and time step are fine enough to resolve the small-scale dynamics in the log layer.

Once the current LES capability in modelling turbulent boundary layers is proved, the synthetic jet is introduced for the interaction study. Although the validation experiments are still in plan and the data are not available yet, we are comfortable with the new simulation since the current LES model is more than capable to model the synthetic jet that is produced at the same operation conditions as in the laminar simulations.

Results and Discussion

The Q-criterion, defined as $Q = (|\Omega|^2 - |S|^2)/2$, is used to define an eddy structure, where Ω is the vorticity tensor and S is the rate-of-strain tensor. In this study, $Q = 0.1$ and $Q = 50$ are selected for laminar and turbulent simulations, respectively, allowing the energetic eddy structures to be captured.

Vortical structures in laminar boundary layer

In figure 5, the instantaneous flow structures are presented with iso-surface of $Q = 0.1$ at Phase $t/T = 60/120$, where Phase $t/T = 0/120$ indicates the diaphragm is at the neutral position with maximum blowing. The dominant eddy structures are highly stretched hairpin vortices which stay in the boundary layer for a distance of $25D_o$ downstream of the orifice. These hairpin vortices are believed to be transformed from vortex-ring-like structures which form during the initial phases [10]. The colour of vorticity magnitudes reveals that the legs of these hairpin vortices are more powerful than their heads. With these hairpin vortices developing downstream, their heads dissipate first. In addition, a pair of secondary streamwise vortical structures form with comparable vorticity magnitudes. The legs of the hairpin vortices and the secondary vortices are very close to the wall, which are believed to be more effective in impacting the near wall flow than the heads of the hairpin vortices.

Figure 6 shows the velocity vectors superimposed on the contours of streamwise vorticity in the wall-normal-spanwise plane $x = 3D_o$ at the same phase as that in figure 5. It can be seen that a pair of secondary streamwise vortices with circulation of

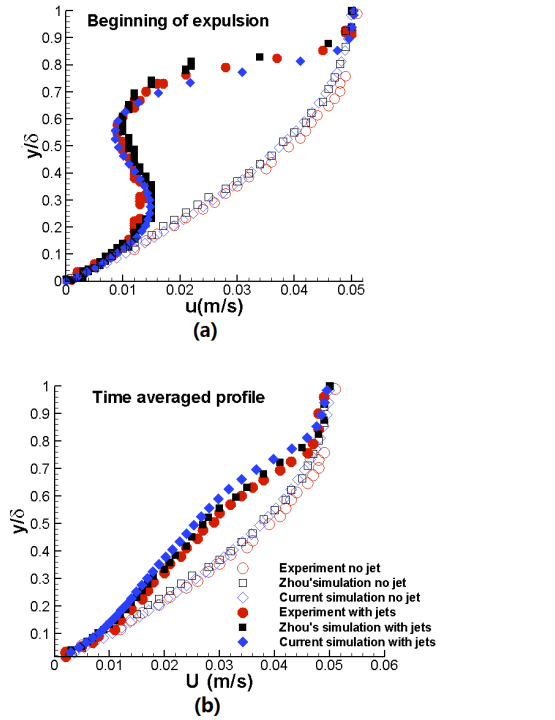


Figure 3. Comparison of (a) phase-averaged and (b) time-averaged velocity profiles at $x = 3D_o$ between the current laminar simulation and the simulations in Zhou and Zhong [10]. δ is the local boundary layer thickness.

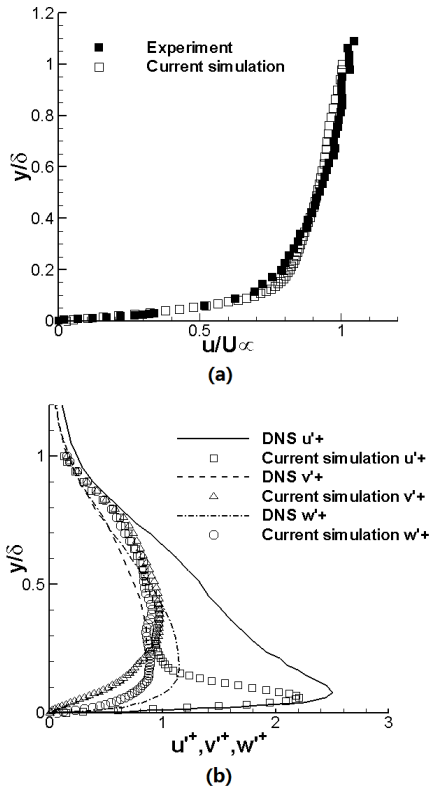


Figure 4. Comparison of time-averaged velocity profiles of a turbulent boundary layer at $x = 0$ (a) mean velocity profiles compared with experimental data and (b) velocity fluctuation profiles compared with DNS results. u^+ , v^+ and w^+ are streamwise, wall-normal and spanwise fluctuations normalized with friction velocity, respectively.

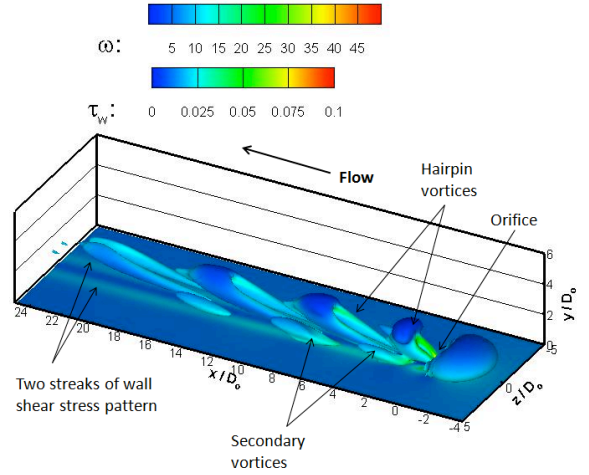


Figure 5. Instantaneous iso-surface of $Q = 0.1$ coloured by vorticity magnitude ω and wall shear stress τ_w pattern in the laminar simulation at Phase $t/T = 60/120$.

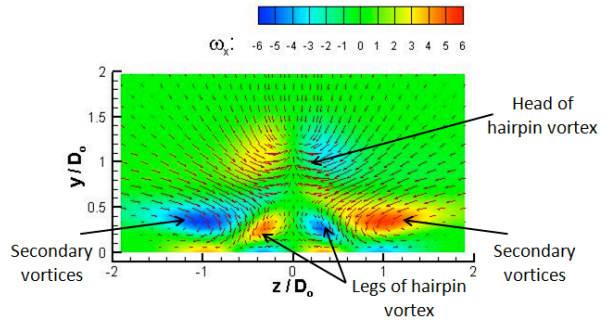


Figure 6. Velocity vectors superimposed on the contours of streamwise vorticity at the wall-normal-spanwise plane $x = 3D_o$ in the laminar simulation at Phase $t/T = 60/120$.

different signs form beside a pair of legs of the hairpin vortex. The velocity vectors clearly reveal that the interaction between these structures induces a downwash motion, which can bring the high-energy fluid in the outer part of the boundary layer into the near-wall region and hence increase the local velocity. And this is further supported by the two streaks of wall shear stress pattern in figure 5.

Vortical structures in turbulent boundary layer

A relatively higher value of $Q = 50$ is used to show the vortical structures generated by a synthetic jet in the turbulent boundary layer. As shown in Figure 7, a highly stretched hairpin vortex is produced just downstream from the orifice. Meanwhile the hairpin vortex produced during the previous diaphragm oscillation cycle experiences fast dissipation and loses its coherent structure very quickly. In addition, the secondary streamwise vortices that are observed in the laminar boundary are not obvious in the current turbulent boundary layer. Phase-averaged velocity vectors and vorticity contours are also used to give more information about these structures as shown in figure 8. Unlike in the laminar boundary layer where the secondary vortices form outboard of the legs of the hairpins, in the current turbulent boundary layer a pair of secondary streamwise vortices forms just beneath the legs of the hairpin vortex, which has also been noticed in [7]. The interaction between the legs of the hairpin vortex and the secondary vortices induces downwash motions in their outboard that bring high-speed fluid into near-wall region. By comparing the contour levels of the vorticity magnitude, it is found that the vortices in the turbulent boundary

layer is much stronger than those in the laminar boundary layer as shown in figures 6 and 8, indicating that synthetic jets in turbulent boundary layers are more effective in mixing enhancement, and hence in the flow separation delay. This is further supported by the time-averaged spanwise distribution of wall shear stress as shown in figure 9.

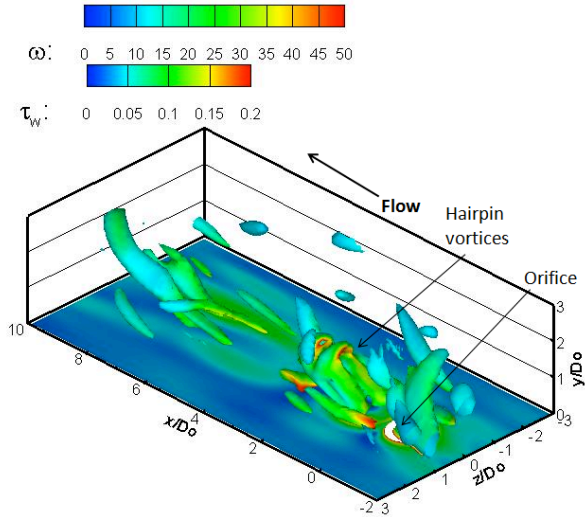


Figure 7. Instantaneous iso-surface of $Q = 50$ coloured by vorticity magnitude ω and wall shear stress τ_w pattern in turbulent simulation at Phase $t/T = 60/120$.

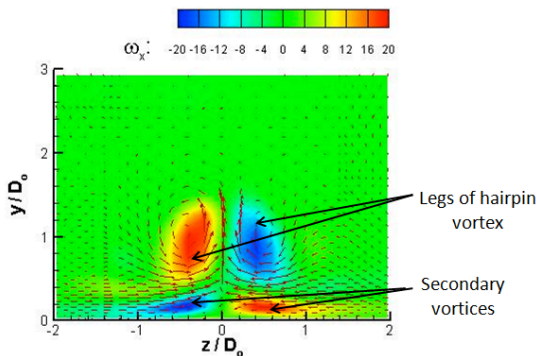


Figure 8. Velocity vectors superimposed on the contours of streamwise vorticity at the wall-normal-spanwise plane $x = 3D_o$ in turbulent simulation at Phase $t/T = 60/120$.

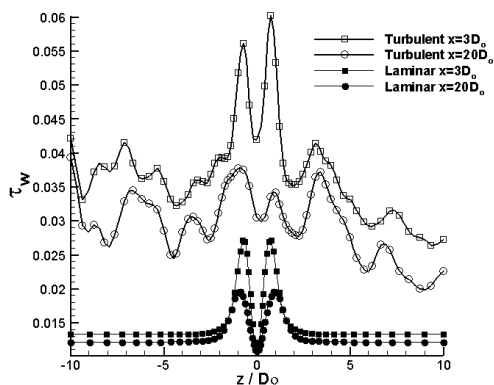


Figure 9. Spanwise distribution of time-averaged wall shear stress at $x = 3D_o$ and $20D_o$.

Conclusions

A circular synthetic jet issued into both laminar and turbulent boundary layers were investigated using 3D CFD simulations.

For turbulent boundary layer simulations, large eddy simulation (LES) was used. The simulation results were validated using existing experimental data and numerical results, and reasonable agreements were achieved.

The instantaneous vortical structures formed by the interaction between the synthetic jet and the laminar and turbulent boundary layers were examined and compared. It is found that the hairpin vortex is the dominated flow structure in both cases. However, there is obvious difference between the two cases in the relative locations of the legs of the hairpin vortices and the secondary streamwise vortices. In addition, the vortices in the turbulent boundary layer are much stronger than that in the laminar boundary layer, indicating that synthetic jets in turbulent boundary layers are more effective in mixing enhancement, and hence in the flow separation delay. Further investigations will be conducted in the near future to obtain a comprehensive understanding of the different behaviours of synthetic jets in laminar and turbulent boundary layers and their different effects on the flow separation control.

Acknowledgement

The authors would like to thank Dr Shan Zhong of University of Manchester for sharing the test data in turbulent boundary layers.

References

- [1] Dandois, J., Garnier, E. & Sagaut, P. Numerical Simulation of Active Separation Control by a Synthetic Jet. *Journal of Fluid Mechanics*, 574. 2007, 25-58.
- [2] Jabbal, M. & Zhong, S. The Near Wall Effect of Synthetic Jets in a Boundary Layer. *International Journal of Heat and Fluid Flow*, 29(1). 2008, 119-130.
- [3] Sergent, E. *Vers une methodologie de couplage entre la Simulation des Grandes Echelles et les modeles statistiques*. PhD thesis, L'Ecole Centrale de Lyon, Lyon, France, 2002.
- [4] Smith, B.L. & Glezer, A. The Formation and Evolution of Synthetic Jets. *Physics of Fluids*, 10(9). 1998, 2281-2297.
- [5] Spalart, P.R., Direct Simulation of a Turbulent Boundary Layer Up to $Re_\theta = 1410$. *Journal of Fluid Mechanics*, 187. 1988, 61-98.
- [6] Zhang, S. & Zhong, S. Experimental Investigation of Flow Separation Control Using an Array of Synthetic Jets. *AIAA Journal*, 48(3). 2010, 611-623.
- [7] Zhang, S. & Zhong, S. Turbulent Flow Separation Control Over a Two-Dimensional Ramp Using Synthetic Jets. *AIAA Journal*, 49(12). 2011, 2637-2649.
- [8] Zhong, S., et al., Towards the Design of Synthetic-jet Actuators for Full-scale Flight Conditions. *Flow, Turbulence and Combustion*, 78(3-4). 2007, 283-307.
- [9] Zhong, S., Millet, F. & Wood, N.J. The Behaviour of Circular Synthetic Jets in a Laminar Boundary Layer. *The Aeronautical Journal*, 2005, 461-470.
- [10] Zhou, J. & Zhong, S. Numerical Simulation of the Interaction of a Circular Synthetic Jet with a Boundary Layer. *Computers & Fluids*, 38(2). 2009, 393-405.
- [11] Ye, T., Qi, S. & Louis, C. Adaptive Feedback Control of Flow Separation. *3rd AIAA Flow Control Conference*, 2006.